doi:10.1017/S1431927620018802
Microsc. Microanal. 26 (Suppl 2), 2020

Atomic Structure and Dynamics of Defects and Grain Boundaries in 2D Pd_2Se_3 Monolayers

Jun Chen[1], Gyeonghee Ryu[1] and Jamie Warner[2]

[1]University of Oxford, Oxford, England, United Kingdom, [2]University of Texas at Austin, Austin, Texas, United States

Abstract: Structural imperfections of 2D crystals such as point vacancies and grain boundaries (GBs) have considerable impacts on their chemical-physical properties. Here we study the atomic structure and dynamics of defects and GBs in monolayer Pd_2Se_3 using annular dark field scanning transmission electron microscopy (ADF-STEM). The Pd_2Se_3 monolayers are reproducibly created by thermally induced phase transformation of few-layered $PdSe_2$ films in an in-situ heating holder in the TEM to promote Se loss. Diverse point vacancies, one-dimensional (1D) defects, GBs and defect ring complexes are directly observed in monolayer Pd_2Se_3, which show a series of dynamics triggered by electron beam. High mobility of vacancies leads to self-healing of point vacancies by migration to the edge and subsequent edge etching under the beam. Specific defects are stabilized by Se−Se bonds, which shift in a staggered way to buffer strain, forming a wave-like 1D defect. Bond rotations are also observed and play an important role in defect and GB dynamics in Pd_2Se_3 during vacancy production. The GBs form in a meandering pathway and migrate by a sequence of Se−Se bond rotations without large scale vacancy formation. In the GB corners and tilted GBs, other highly symmetric vacancy defects also occur to adapt to the orientation change. These results give atomic level insights into the defects and GBs in Pd_2Se_3 2D monolayers.

2D materials have expanded rapidly beyond graphene over the past few years.[1-3] The semiconducting transition metal dichalcogenides (TMDs, e.g MoS_2) have advanced hugely in the opto-electronics using all 2D materials.[4-9] Further development, though, requires continual investigation of new 2D materials systems beyond those that are well known. Moreover, creating scalable methods to make new monolayers that do not exist as bulk layered materials provides access to new crystals yet to be fully explored. Recently, it was found that electron beam irradiation can help transform few-layered $PdSe_2$ into monolayered regions of Pd_2Se_3 crystals.[10-11] This novel semiconducting Pd_2Se_3 monolayers are not found as bulk layered system. Meanwhile, device applications of new 2D materials require atomic understanding of their structures, particularly their defects such as point vacancies and GBs. [12-16] However, defects in monolayer Pd_2Se_3 have yet to be systematically studied mainly due to the novelty of the material and the difficulty in material production. While new crystal phases can be created by electron beam irradiation, it does not provide scalable production techniques to advance the applications.

Here, we produce Pd_2Se_3 monolayers scalably from commercial few-layered $PdSe_2$ by using thermal annealing in an in-situ heating stage in STEM (Fig. 1a-b), which can precisely monitor the phase-change temperature of the material. The interlayer fusion of $PdSe_2$ was triggered by thermal energy at 350 and the structural reconstruction results from the Se atom loss (Fig. 1c-f).

Various point defects in Pd_2Se_3 are constructed from dumbbell Se vacancies ($V-Se_B$) and adatoms (Fig. 1g-j), including the cross-shape defect (Fig. 1k-o) and the composite defect of $V-Se_B$ with Se adatom (Fig. 1p-t). The fast dynamics suggest high mobility of Se vacancies. The $V-Se_B$ was finally repaired by capturing an extra Se probably coming from the gradually consumed edge, showing a self-healing phenomenon (Fig. 1t). The edge was etched due to the beam spluttering and the fast vacancy migration to the edge, differing from the Mo- or W based TMDs, which often form line vacancies or holes with numerous vacancies produced, suggesting the possibly lower migrating energy of Se vacancies in Pd_2Se_3.

GBs can often form in two differently oriented grains in 2D crystals. Fig. 2a-g shows the dynamics of the meandering 90°GBs with stepped kinks between two perpendicular Pd_2Se_3 grains (Fig. 2d-g). The GB defect

units are different from those in graphene, h-BN or other hexagonal MX_2 TMDs connected by dislocation cores. Here the GB defects maintain the stoichiometry and can be created by 90° bond rotation of the covalent Se_B–Se_B bond without losing atoms (Fig. 2k). Unlike the typical hexagonal TMDs, the existence of Se_B–Se_B in Pd_2Se_3 facilitates the Stone-Wales bond rotation, making it a significant process in its GB formation and dynamics. Under the beam, the 90° GB migrated with the climb of the GB steps (Fig. 2d-e) through the Se_B–Se_B bond rotation. This GB migration mechanism differs from that in other TMDs which involves mobile S vacancies/adatoms and significant lattice reconstruction. Apart from this, the 90° GBs can be created from pristine Pd_2Se_3 monolayers when partial lattices inverted with collective 90° bond rotation of a group of Se_B–Se_B triggered by electron beam (Fig. 2n-o), after which a chain of GB defect units are produced (Fig. 2q,u,t).

The common line vacancies in TMDs were not observed in Pd_2Se_3. Instead a distinctive wave-like one-dimensional structure with local compressive strain was noticed which has reversible transformation under the beam. This flexible structure makes Pd_2Se_3 adaptable to local strains during beam-induced kinetic process.

We also found a type of metastable peculiar defect rings at Pd_2Se_3 monolayer with fast electron-driven dynamics. These defect loops appear with intricate interplay with the sub-nanopores, serving as the bridging structure before the lattice breaks. The flexible bonding between Pd and Se atoms have rendered this unique and variable defect ring, which is quite uncommon among the typical TMDs.

In short, the defects and GBs in the Pd_2Se_3 monolayers present diversity, adaptability and abundant electron-induced dynamics. This can enrich the structural knowledge of 2D materials. It is expected that manipulating varieties of defects in Pd_2Se_3 would offer approaches to controlling the transport characteristics or solar absorption features of Pd_2Se_3-based (opto-)electronic devices.

https://doi.org/10.1017/S1431927620018802 Published online by Cambridge University Press

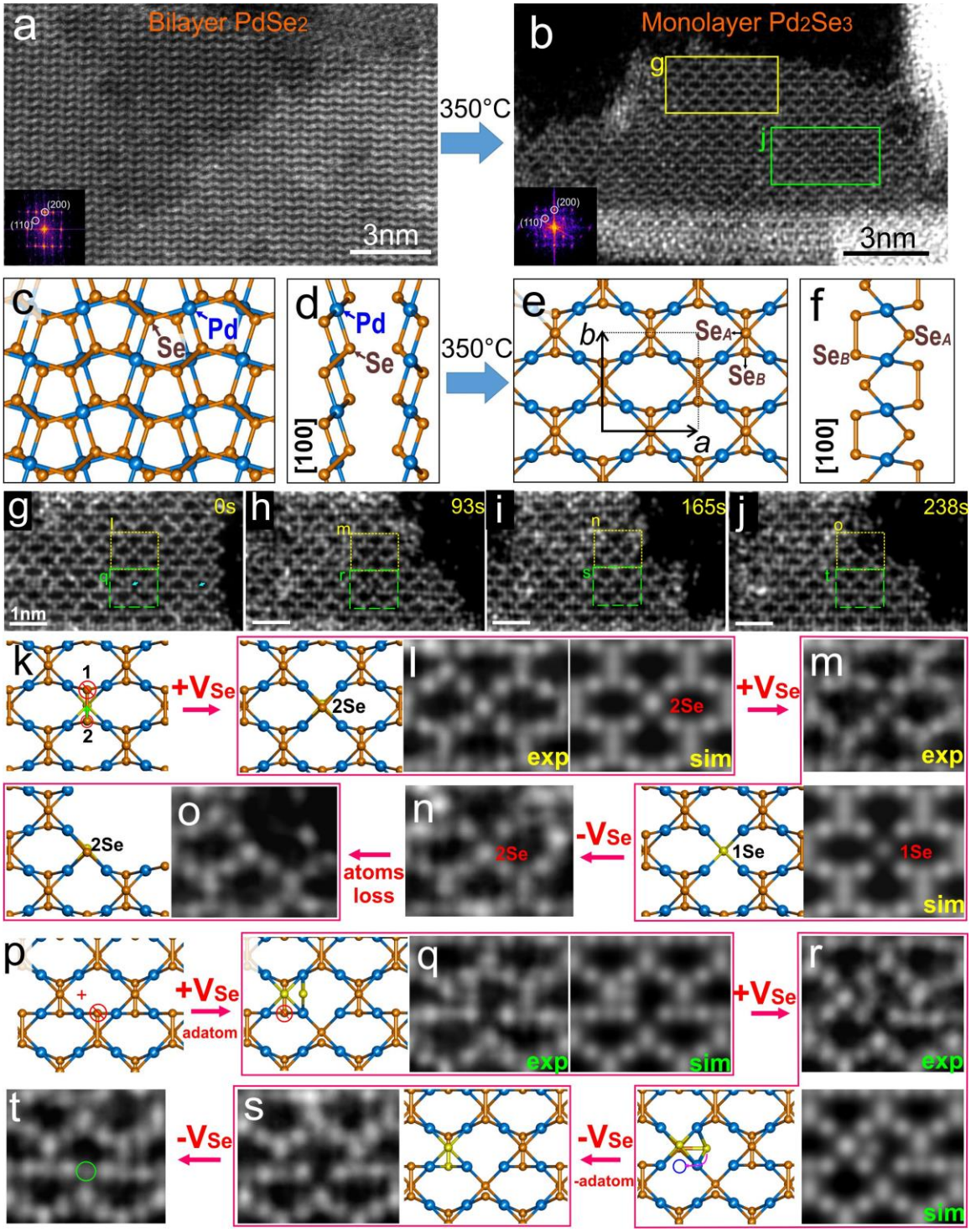

Figure 1. (a, b) ADF-STEM images showing the transformation from (a) a few-layer PdSe2 film to (b) monolayer Pd2Se3 when treated by in situ heating at 350 °C. Insets are the corresponding power spectra of FFT of the images. (c, d) Atomic model (Pd, cyan; Se, yellow) of the bilayer PdSe2 of the front and side views. (e, f) Atomic model of the monolayer Pd2Se3 of the front and side views. (g-j) Time-series ADF-STEM images showing the point defects and edge dynamics of monolayer Pd2Se3. (k–t) Structures and dynamics of point defects and adatoms in Pd2Se3 monolayers. (k–o) Dynamical process and mechanism of the cross-shape point defect caused by Se vacancies in a small region shown by magnified ADF-STEM images and corresponding

https://doi.org/10.1017/S1431927620018802 Published online by Cambridge University Press

atomic model. (p–t) Dynamics of the point defect with an adatom in a small region shown by magnified ADF-STEM images and corresponding atomic model illustration.

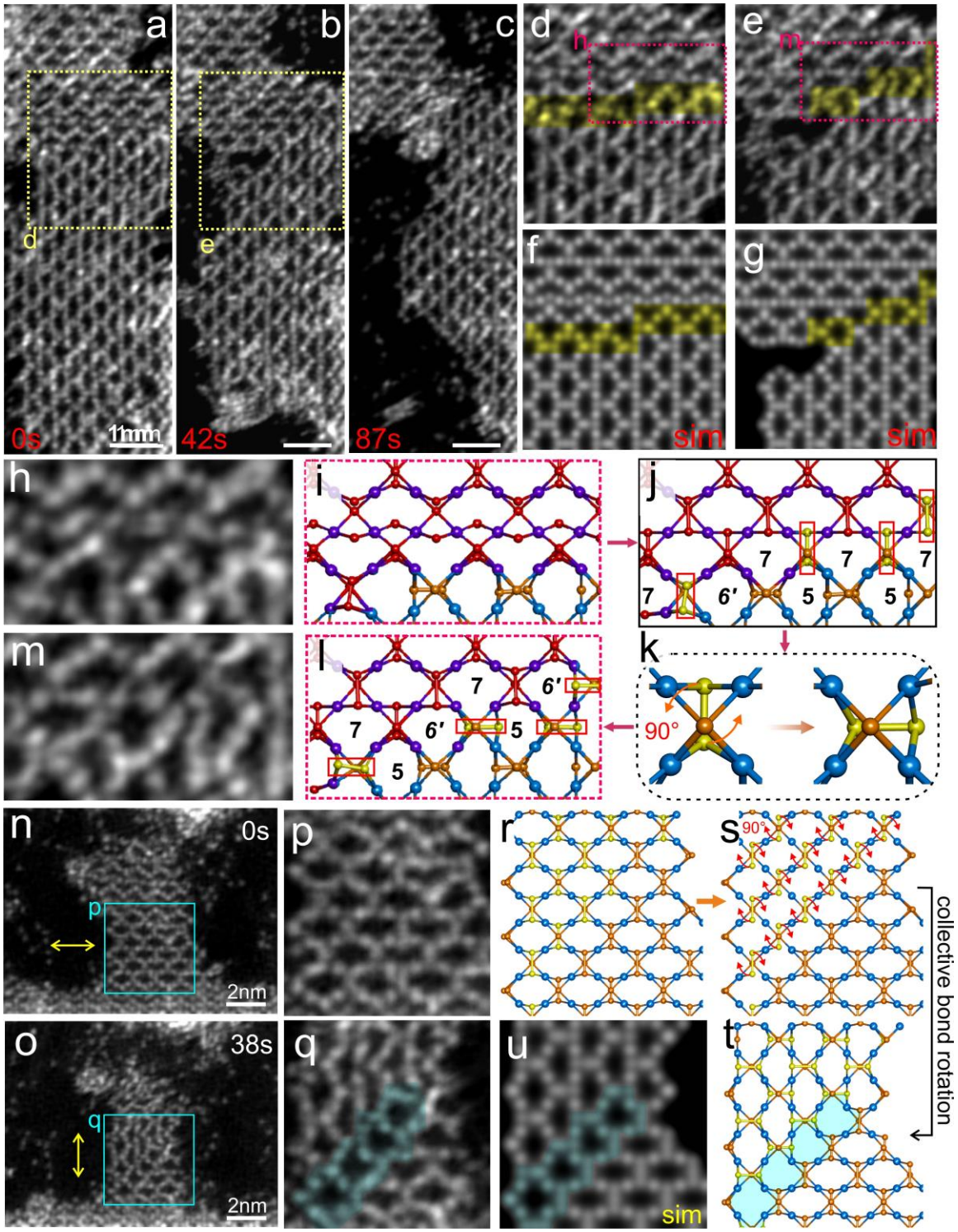

Figure 2. (a-c) ADF-STEM image sequence of a Pd2Se3 monolayer region with 90° grain boundaries (GBs). (d,e) Magnified views of the yellow boxed regions in (a,b) respectively with yellow colour highlighting the GB region, (f,g) multislice simulated ADF-STEM images. (h,m) Magnified views of the yellow boxed regions in (d,e) with (i,l) corresponding atomic models. (j,k) Scheme showing the GB migration mechanism through

https://doi.org/10.1017/S1431927620018802 Published online by Cambridge University Press

90° bound rotation. (n,o) ADF-STEM image sequence showing the orientation inversion of partial Pd2Se3 grain accompanied by GB formation under electron beam stimulation. (p,q) Enlarged views of the blue boxed regions in (n,o). (r-t) Schematic atomic illustration of the evolution mechanism of the grain orientation inversion by collective 90° bond rotation. (h) Simulated ADF-STEM image corresponding to (q). The blue colour in (q,u,t) highlights the GB defects.

References

[1] Z. Liu,S.P. Lau,F. Yan, *Chem. Soc. Rev.* **2015,** *44*, 5638-5679.
[2] C. Tan,X. Cao,X.-J. Wu,Q. He,J. Yang,X. Zhang,J. Chen,W. Zhao,S. Han,G.-H. Nam, *Chem. Rev.* **2017,** *117*, 6225-6331.
[3] J.S. Lee,S.H. Choi,S.J. Yun,Y.I. Kim,S. Boandoh,J.-H. Park,B.G. Shin,H. Ko,S.H. Lee,Y.-M. Kim,Y.H. Lee,K.K. Kim,S.M. Kim, *Science* **2018,** *362*, 817-821.
[4] S. Manzeli,D. Ovchinnikov,D. Pasquier,O.V. Yazyev,A. Kis, *Nat. Rev. Mater.* **2017,** *2*, 17033.
[5] Q.H. Wang,K. Kalantar-Zadeh,A. Kis,J.N. Coleman,M.S. Strano, *Nat. Nanotechnol.* **2012,** *7*, 699-172.
[6] B. Radisavljevic,A. Radenovic,J. Brivio,i.V. Giacometti,A. Kis, *Nat. Nanotechnol.* **2011,** *6*, 147-150.
[7] X. Duan,C. Wang,A. Pan,R. Yu,X. Duan, *Chem. Soc. Rev.* **2015,** *44*, 8859-8876.
[8] R. Kappera,D. Voiry,S.E. Yalcin,B. Branch,G. Gupta,A.D. Mohite,M. Chhowalla, *Nat. Mater.* **2014,** *13*, 1128–1134.
[9] K.F. Mak,C. Lee,J. Hone,J. Shan,T.F. Heinz, *Phys. Rev. Lett.* **2010,** *105*, 136805.
[10] J. Lin,S. Zuluaga,P. Yu,Z. Liu,S.T. Pantelides,K. Suenaga, *Phys. Rev. Lett.* **2017,** *119*, 016101.
[11] Z. Sebastian,L. Junhao,S. Kazu,T.P. Sokrates, *2D Mater.* **2018,** *5*, 035025.
[12] W. Zhou,X. Zou,S. Najmaei,Z. Liu,Y. Shi,J. Kong,J. Lou,P.M. Ajayan,B.I. Yakobson,J.-C. Idrobo, *Nano Lett.* **2013,** *13*, 2615-2622.
[13] S. Wang,A. Robertson,J.H. Warner, *Chem. Soc. Rev.* **2018,** *47*, 6764-6794.
[14] A.M. van der Zande,P.Y. Huang,D.A. Chenet,T.C. Berkelbach,Y. You,G.H. Lee,T.F. Heinz,D.R. Reichman,D.A. Muller,J.C. Hone, *Nat. Mater.* **2013,** *12*, 554–561.
[15] S. Barja,S. Wickenburg,Z.-F. Liu,Y. Zhang,H. Ryu,Miguel M. Ugeda,Z. Hussain,Z.-X. Shen,S.-K. Mo,E. Wong,Miquel B. Salmeron,F. Wang,M.F. Crommie,D.F. Ogletree,Jeffrey B. Neaton,A. Weber-Bargioni, *Nat. Phys.* **2016,** *12*, 751–756.
[16] Y.L. Huang,Y. Chen,W. Zhang,S.Y. Quek,C.-H. Chen,L.-J. Li,W.-T. Hsu,W.-H. Chang,Y.J. Zheng,W. Chen,A.T.S. Wee, *Nat. Commun.* **2015,** *6*, 6298.

https://doi.org/10.1017/S1431927620018802 Published online by Cambridge University Press